Journal of Mathematical Sciences and Modelling, 6(3) (2023) 105-119
Research Article

Journal of Mathematical Sciences and Modelling

Journal Homepage: www.dergipark.gov.tr/jmsm
ISSN 2636-8692
DOI: http://dx.doi.org/10.33187/jmsm.1126660

Implementation of the Hybrid ADI-FDTD Scheme to Maxwell Equation for Mathematical Modeling of Breast Tumor

Ümmü Şahin Şener

Department of Mathematics, Faculty of Science and Arts, Kırklareli University, Kırklareli, Türkiye

Article Info

Keywords: *ADI-FDTD, Breast tumor, FDTD, Mathematical modeling, Maxwell equations, Scattered field*
2010 AMS: *35L05, 35-04*
Received: *6 June 2022*
Accepted: *9 June 2023*
Available online: *31 July 2023*

Abstract

Breast cancer is the most common cancer in women, and non-destructive detection of the tumor is vital. The interaction of electromagnetic waves with breast tissue and the behavior of waves after interaction are used to model tumor detection mathematically. The behavior of electromagnetic waves in a medium is described using Maxwell's equations. Electromagnetic waves propagate according to the electrical properties of a medium. Since the electrical properties of tumor tissue are different from those of normal breast tissue, it is assumed that the tumor is a lossy dielectric sphere, and the breast is a lossy dielectric medium. Under this assumption, Maxwell's equations are used to calculate the scattered field from the tumor. The field scattered by the tumor is different from other tissues because their dielectric properties are different. The location and size of the tumor can be determined by utilizing the difference in scattering from the tissues. While the scattering field from the tumor in spherical geometric form is analytically calculated, it is not analytically possible to calculate the scattering field from the tumor in different geometric shapes. In addition to non-destructive detection of the tumor, an efficient numerical method, the finite difference time domain method (FDTD), is used to simulate the field distribution. After the location of the tumor is determined, the Alternating Direction Implicit (ADI) FDTD method, which gives simulation results by dividing the computation domain into smaller sub-intervals, can be used. Scattered fields are calculated analytically in the geometry where the tumor is in the form of a smooth sphere, and in more complex geometry, the field distributions are successfully obtained with the help of MATLAB using FDTD and ADI-FDTD algorithms.

1. Introduction

According to 2019 World Health Organization (WHO) estimates, cancer is the first or second leading cause of death before age 70 in 112 of 183 countries and is the most important factor negatively affecting longevity and healthy living [1–3]. Among the cancer cases detected, breast cancer is the most common cancer. In 2020, 2.3 million new cases of breast cancer will be detected. This number represents 11.7% of all cancer cases [4], and it is estimated that the risk of cancer will increase in the coming years. As with many other types of cancer, breast cancer does not show symptoms in its early stages, but early diagnosis and treatment prolongs the survival of patients, reduces recurrences, and increases the patient's life expectancy [5–7]. Therefore, detection of breast cancer at the initial stage is important for the success of the treatment. X-ray mammography, ultrasound scanning, and magnetic resonance imaging (MRI) are clinical imaging modalities commonly used in breast cancer detection [8–10].

X-ray mammography has some limitations, especially in young women with particularly dense breast tissue who have never had breast cancer. Other disadvantages of X-ray mammography can be listed as increasing the possibility of getting cancer due to the use of ionizing radiation, discomfort, and pain due to the presence of breast compression and causing concern in patients due to false negative and false positive results [11–13]. The ultrasound method uses sound waves that are converted into pulses by means of a transducer. In cases where a certain feature of the tissue is different in the waves sent to the breast tissue, reflections called echoes occur between tissues with different

Email address and ORCID number: **ummusahin@klu.edu.tr, 0000-0001-9055-8734**
Cite as "Ü. Şahin Şener, *Implementation of the hybrid ADI-FDTD scheme to Maxwell equation for mathematical modeling of breast tumor*, J. Math. Sci. Model., 6(3) (2023), 105-119"

characteristics and form ultrasound images. This method is more costly than X-ray mammography, and the images obtained are also low resolution. Although the MRI technique is more expensive than the ultrasound method and X-ray mammography and cannot determine the exact location of the tumors, it can be used in patients with dense breast tissue and can detect even small tumors [14].
In order to overcome the limitations and disadvantages of MRI imaging, ultrasound method and X-ray method, microwave imaging technique, which uses data obtained from the interaction of electromagnetic waves and tissues, is used. The microwave imaging method has advantages such as using non-ionized waves, not damaging the tissues, inexpensive, and comfortable of use [15]. Normal breast tissue and malignant tissues have different dielectric properties, and this method takes advantage of the dielectric contrast between these tissues. When breast tissue interacts with microwaves, weaker responses from benign lesions are expected, while stronger responses from malignancies are expected during imaging [16–21].
Assuming that the tumor in the breast tissue is spherical, our problem turns into the problem of scattering of electromagnetic waves by a dielectric sphere. The scattering and propagation of the electromagnetic wave from the dielectric sphere can be solved analytically [22, 23]. However, since the tumor is not always be in the shape of a regular sphere, it is not possible to solve the electromagnetic field distribution analytically in a complex geometry. In this case, it is necessary to solve the problem numerically. The modeling of the interaction between electromagnetic waves at microwave frequencies and breast tissue can be done by the numerical solution of Maxwell's equations [24, 25]. Since the FDTD method is one of the most commonly used methods in algorithms for simulating breast imaging at microwave frequencies, the time-dependent Maxwell equations are solved using this method [26].
Although the FDTD method is a commonly used method for solving electromagnetic simulation problems, the maximum time step size should not exceed the minimum cell size in the computational domain (Courant-Friedrich-Levy (CFL) condition), since the traditional FDTD method is an open finite difference algorithm. The maximum size of the time step should be limited by the maximum propagation velocity and the minimum cell size in the computation domain [27]. When the computational domain is transformed into a fine geometry, i.e., when the cell size becomes smaller, it becomes difficult to satisfy the stability condition in the traditional FDTD method. Therefore, a solution can be found using the alternative directionally implicit finite difference time domain method (ADI-FDTD), which is one of the unconditionally stable FDTD methods [28–32].
Since electromagnetic wave propagation and scattering problems are open problems and the FDTD algorithm must be terminated after a certain step, the computation domain is truncated after sufficient interaction with the breast tissue is achieved. Boundary conditions are used where the computation domain is truncated [33, 34]. Boundary conditions should be determined established to prevent waves from returning to the computation domain when they reach the boundary by propagating in the breast tissue. Since the equivalent for open problems in numerical computations is an infinite computation domain, the real infinity of space can be modeled by truncating the computation domain somewhere and applying Absorbing Boundary Conditions (ABC). ABCs are obtained by using absorber lossy media. The use of absorber materials as absorber boundary conditions started with the use of classical lossy and nondispersive materials. The perfectly matched layer developed by Berenger is the strongest ABC compared to other methods. The perfectly matched layer (PML) is a lossy material boundary layer with a thickness of a few cells that surrounds the computational domain from the truncated region. The PML boundary layer matches up with perfectly to the computational domain [35]. PML uses artificial structural parameters to establish the wave impedance matching condition, regardless of the frequency and angle of the incident wave. In our study, it is assumed that the computation domain is surrounded by the PML [36].
In this study, first of all, since the tumor in the breast tissue is considered to be spherical and the spherical structure is a regular geometric shape, an analytical examination of the interaction of electromagnetic wave and a lossy dielectric sphere will be given. Secondly, two different breast simulation geometries will be created, and numerical solution will be made in the geometry where it is not possible to analyze the electromagnetic wave-tissue interaction analytically using the traditional FDTD method. The last but not least it is planned to obtain a better simulation result by simulating with the traditional FDTD method and dividing the part determined to be a tumor into smaller cells and applying the ADI-FDTD algorithm to the area where the smaller cells are located.

2. Material and Methods

2.1. Analytical study

Suppose that the electric field of a uniform plane wave propagating along the z-axis and polarized in the x-direction, as shown in Figure 2.1a and Figure 2.1b, the electric field and magnetic field of the incident wave on a sphere can be expressed as follows:

$$\mathbf{E}^i = \hat{\mathbf{a}}xEx^i = \hat{\mathbf{a}}xE0e^{-j\beta z} = \hat{\mathbf{a}}xE0e^{-j\beta r\cos\theta} \tag{2.1}$$

$$\mathbf{H}^i = \hat{\mathbf{a}}_y H_y^i = \hat{\mathbf{a}}_y H_0 e^{-j\beta z} = \hat{\mathbf{a}}_y H_0 e^{-j\beta r\cos\theta}$$

By transforming from rectangular coordinate components to spherical coordinate components using the equality as follows: By transforming from rectangular coordinate components to spherical coordinate components using the equality as follows:

$$x = r\sin\theta\cos\phi,\ y = r\sin\theta\sin\phi,\ z = r\cos\theta \tag{2.2}$$

Using Eq. (2.2), the relationship between rectangular and spherical components can be written as:

$$\begin{aligned} A_r &= A_x\sin\theta\cos\phi + A_y\sin\theta\sin\phi + A_z\cos\theta \\ A_\theta &= A_x\cos\theta\cos\phi + A_y\cos\theta\sin\phi - A_z\sin\theta \\ A_\phi &= -A_x\sin\phi + A_y\cos\phi \end{aligned} \tag{2.3}$$

Using the system (2.3) the x-component of the Eq. (2.1) can be express in spherical components to

$$\mathbf{E}^i = \hat{\mathbf{a}}_r E_r^i + \hat{\mathbf{a}}_\theta E_\theta^i + \hat{\mathbf{a}}_\phi E_\phi^i$$

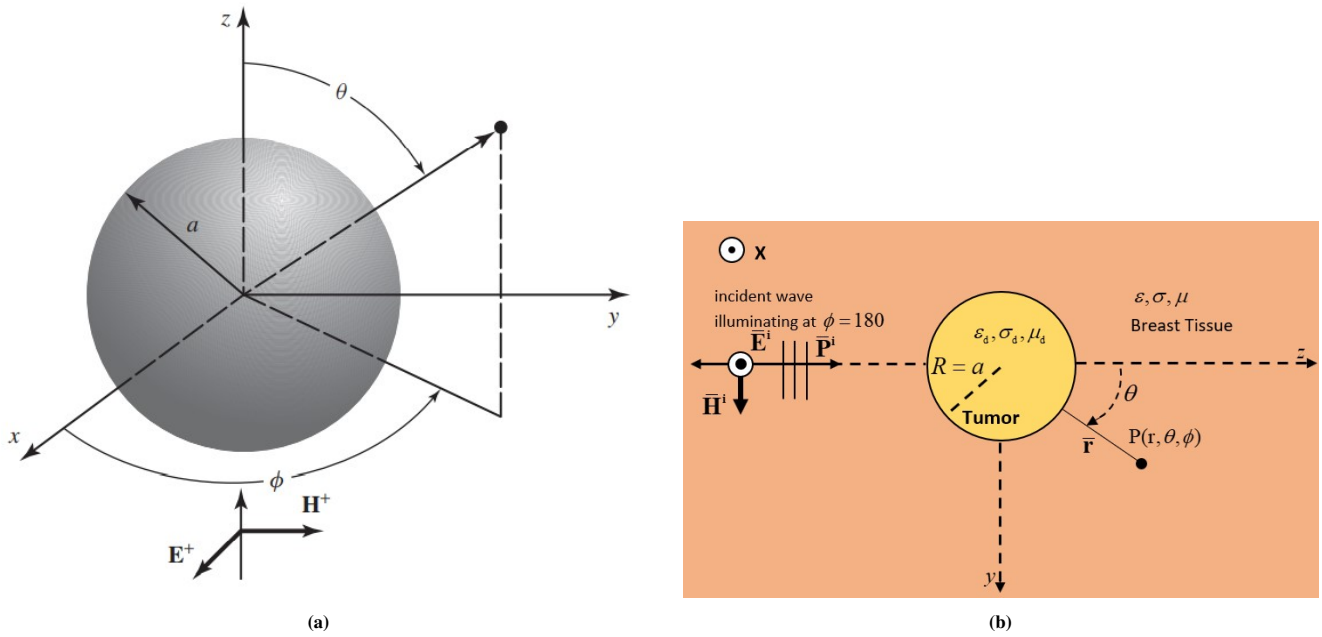

Figure 2.1: (a) Uniform plane wave incident on a sphere [22] **(b)** The state of the electromagnetic wave that incident on a lossy and dispersive dielectric tumor in a lossy and dispersed breast tissue [23]

$$\begin{aligned} E_r^i &= E_x^i \sin\theta\cos\phi = E_0 \sin\theta\cos\phi e^{-j\beta r\cos\theta} = E_0 \frac{\cos\phi}{j\beta r}\frac{\partial}{\partial\theta}\left(e^{-j\beta r\cos\theta}\right) \\ E_\theta^i &= E_x^i \cos\theta\cos\phi = E_0 \cos\theta\cos\phi e^{-j\beta r\cos\theta} \\ E_\phi^i &= -E_x^i \sin\phi = -E_0 \sin\phi e^{-j\beta r\cos\theta} \end{aligned}$$

All of the spherical components of the incident electric field can be expressed using the $E_x^+ = e^{-j\beta z} = e^{-j\beta r\cos\theta} = \sum_{n=0}^{\infty} a_n j_n(\beta r) P_n(\cos\theta)$ equality. In this equality $a_n = j^{-n}(2n+1)$.

$$\begin{aligned} E_r^i &= E_0 \frac{\cos\phi}{j\beta r}\sum_{n=0}^{\infty} j^{-n}(2n+1)\, j_n(\beta r)\frac{\partial}{\partial\theta}\left(P_n(\cos\theta)\right) \\ E_\theta^i &= E_0 \cos\theta\cos\phi \sum_{n=0}^{\infty} j^{-n}(2n+1)\, j_n(\beta r) P_n(\cos\theta) \\ E_\phi^i &= -E_0 \sin\phi \sum_{n=0}^{\infty} j^{-n}(2n+1)\, j_n(\beta r) P_n(\cos\theta) \end{aligned} \tag{2.4}$$

The following Eq. (2.5) can be written between the Bessel and Legendre functions.

$$\begin{aligned} j_n(\beta r) &= \frac{1}{\beta r}\hat{J}_n(\beta r) \\ \frac{\partial P_n}{\partial\theta} &= P_n^1(\cos\theta) \\ P_0^1 &= 0 \end{aligned} \tag{2.5}$$

The Eq. (2.4) can be written as in Eq. (2.6) using the Eq. (2.5)

$$\begin{aligned} E_r^i &= -jE_0 \frac{\cos\phi}{(\beta r)^2}\sum_{n=1}^{\infty} j^{-n}(2n+1)\hat{J}_n(\beta r) P_n^1(\cos\theta) \\ E_\theta^i &= E_0 \frac{\cos\theta\cos\phi}{\beta r}\sum_{n=0}^{\infty} j^{-n}(2n+1)\hat{J}_n(\beta r) P_n^0(\cos\theta) \\ E_r^i &= -E_0 \frac{\sin\phi}{\beta r}\sum_{n=0}^{\infty} j^{-n}(2n+1)\hat{J}_n(\beta r) P_n^0(\cos\theta) \end{aligned} \tag{2.6}$$

Using the vector potential A_i^r the incident electric field can be written as in the Eq. (2.7).

$$E_r^i = \frac{1}{j\omega\mu\varepsilon}\left(\frac{\partial^2}{\partial r^2} + \beta^2\right) A_r^i \tag{2.7}$$

By equating Eq. (2.7) with Eq. (2.6), the following equation can be written for A_r^i.

$$E_r^i = \frac{1}{j\omega\mu\varepsilon}\left(\frac{\partial^2}{\partial r^2}+\beta^2\right)A_r^i$$

TE and TM (with respect to r) fields are formed by vector potentials $\mathbf{A}$ and $\mathbf{F}$. TE mode fields are produced by taking $\mathbf{A}=0$, $\mathbf{F}=\hat{\mathbf{a}}_r F_r(r,\theta,\phi)$, and TM mode fields are produced by writing $\mathbf{A}=\hat{\mathbf{a}}_r A_r(r,\theta,\phi)$, $\mathbf{F}=0$. In addition, the incident and scattered fields by the sphere can be expressed as a superposition of TE and TM [22]. Studies on the scattering and propagation of fields by a lossy dielectric sphere have emerged from the investigation of the interaction of the perfect electric conductor (PEC) sphere and waves. In the lossy dielectric sphere, unlike the PEC sphere, waves penetrate the sphere. Boundary conditions are used to establish a relationship between the fields outside and inside the sphere. Tangential electric and magnetic fields are continuous in a lossy dielectric sphere. To develop the governing equations for the lossy dielectric sphere the geometry is used given in Figure 2.1b. It is accepted that the medium outside the sphere is free space and wave number is β_0, the inside of the sphere is lossy dielectric medium and wave number is $\dot{\beta}_0$. The relative complex permittivity of the dielectric medium $\dot{\varepsilon}_r\,(\dot{\varepsilon}_r=\varepsilon_r{}'-j\varepsilon_r{}'')$ and complex permeability $\dot{\mu}_r\,(\dot{\mu}_r=\mu_r{}'-j\mu_r{}'')$.
The total, incident and scattered fields outside the sphere can be represented by the vector potentials in terms of series expansion given by the follows:

$$\begin{aligned}
A_r^{t+} &= A_r^i + A_r^s = E_0\frac{\cos\phi}{\omega}\sum_{n=1}^{\infty}\left[a_n\hat{J}_n(\beta r)+b_n\hat{H}_n^{(2)}(\beta r)\right]P_n^1(\cos\theta)\\
F_r^{t+} &= F_r^i + F_r^s = E_0\frac{\sin\phi}{\omega\eta}\sum_{n=1}^{\infty}\left[a_n\hat{J}_n(\beta r)+c_n\hat{H}_n^{(2)}(\beta r)\right]P_n^1(\cos\theta)\\
a_n &= j^{-n}\frac{(2n+1)}{n(n+1)}
\end{aligned}$$

The corresponding electric field and magnetic fields to these potentials are given below.

$$\begin{aligned}
E_r^t &= \frac{1}{j\omega\mu\varepsilon}\left(\frac{\partial^2}{\partial r^2}+\beta^2\right)A_r^t\\
E_\theta^t &= \frac{1}{j\omega\mu\varepsilon}\frac{1}{r}\frac{\partial^2 A_r^t}{\partial r\partial\theta}-\frac{1}{\varepsilon}\frac{1}{r\sin\theta}\frac{\partial F_r^t}{\partial\phi}\\
E_\phi^t &= \frac{1}{j\omega\mu\varepsilon}\frac{1}{r\sin\theta}\frac{\partial^2 A_r^t}{\partial r\partial\phi}+\frac{1}{\varepsilon}\frac{1}{r}\frac{\partial F_r^t}{\partial\theta}
\end{aligned}$$

$$\begin{aligned}
H_r^t &= \frac{1}{j\omega\mu\varepsilon}\left(\frac{\partial^2}{\partial r^2}+\beta^2\right)F_r^t\\
H_\theta^t &= \frac{1}{\mu}\frac{1}{r\sin\theta}\frac{\partial A_r^t}{\partial\phi}+\frac{1}{j\omega\mu\varepsilon}\frac{1}{r}\frac{\partial^2 F_r^t}{\partial r\partial\theta}\\
H_\phi^t &= -\frac{1}{\mu}\frac{1}{r}\frac{\partial A_r^t}{\partial\theta}+\frac{1}{j\omega\mu\varepsilon}\frac{1}{r\sin\theta}\frac{\partial^2 F_r^t}{\partial r\partial\phi}
\end{aligned}$$

Although the vector potentials inside and outside the sphere are similar, waves propagating outside the sphere are used, while standing waves in the radial direction are used inside the sphere. Consequently, the vector potentials for the total fields inside the sphere can be written as:

$$\begin{aligned}
A_r^{t-} &= E_0\frac{\cos\phi}{\omega}\sum_{n=1}^{\infty}d_n\hat{J}_n\left(\dot{\beta}_d r\right)P_n^{(1)}(\cos\theta)\\
F_r^{t-} &= E_0\frac{\sin\phi}{\omega\dot{\eta}}\sum_{n=1}^{\infty}e_n\hat{J}_n\left(\dot{\beta}_d r\right)P_n^{(1)}(\cos\theta)
\end{aligned}$$

b_n, c_n coefficients for the fields outside the sphere and d_n, e_n for the fields inside the sphere can be obtained by applying the boundary conditions. In the case of $(r\le a)$, the vector potentials on and inside the sphere are considered, and (-) superscript is used, while $(r\ge a)$ the (+) symbol is used on the potentials, taking into account the vector potentials on and outside the sphere and the fields associated with these potentials [22]. By using boundary conditions given the equations below, the coefficients b_n, c_n, d_n and e_n depending on a_n can be obtained as follows:

$$\begin{aligned}
E_\theta^{t-}(r=a,0\le\theta\le\pi,0\le\phi\le2\pi) &= E_\theta^{t+}(r=a,0\le\theta\le\pi,0\le\phi\le2\pi)\\
E_\phi^{t-}(r=a,0\le\theta\le\pi,0\le\phi\le2\pi) &= E_\phi^{t+}(r=a,0\le\theta\le\pi,0\le\phi\le2\pi)\\
H_\theta^{t-}(r=a,0\le\theta\le\pi,0\le\phi\le2\pi) &= H_\theta^{t+}(r=a,0\le\theta\le\pi,0\le\phi\le2\pi)\\
H_\phi^{t-}(r=a,0\le\theta\le\pi,0\le\phi\le2\pi) &= H_\phi^{t+}(r=a,0\le\theta\le\pi,0\le\phi\le2\pi)
\end{aligned}$$

$$
\begin{aligned}
b_n &= \frac{-\sqrt{\dot{\varepsilon}_r}\hat{J}_n'(\beta_0 a)\hat{J}_n\left(\dot{\beta}_d a\right)+\sqrt{\dot{\mu}_r}\hat{J}_n(\beta_0 a)\hat{J}_n'\left(\dot{\beta}_d a\right)}{\sqrt{\dot{\varepsilon}_r}H_n^{(2)'}(\beta_0 a)\hat{J}_n\left(\dot{\beta}_d a\right)+\sqrt{\dot{\mu}_r}H_n^{(2)}(\beta_0 a)\hat{J}_n'\left(\dot{\beta}_d a\right)}a_n \\
c_n &= \frac{-\sqrt{\dot{\varepsilon}_r}\hat{J}_n(\beta_0 a)\hat{J}_n'\left(\dot{\beta}_d a\right)+\sqrt{\dot{\mu}_r}\hat{J}_n'(\beta_0 a)\hat{J}_n\left(\dot{\beta}_d a\right)}{\sqrt{\dot{\varepsilon}_r}H_n^{(2)}(\beta_0 a)\hat{J}_n'\left(\dot{\beta}_d a\right)-\sqrt{\dot{\mu}_r}H_n^{(2)'}(\beta_0 a)\hat{J}_n\left(\dot{\beta}_d a\right)}a_n \\
d_n &= -j\frac{\dot{\mu}_r\sqrt{\dot{\varepsilon}_r}}{\sqrt{\dot{\varepsilon}_r}H_n^{(2)'}(\beta_0 a)\hat{J}_n\left(\dot{\beta}_d a\right)-\sqrt{\dot{\mu}_r}H_n^{(2)}(\beta_0 a)\hat{J}_n'\left(\dot{\beta}_d a\right)}a_n \\
e_n &= j\frac{\dot{\mu}_r\sqrt{\dot{\varepsilon}_r}}{\sqrt{\dot{\varepsilon}_r}H_n^{(2)}(\beta_0 a)\hat{J}_n'\left(\dot{\beta}_d a\right)-\sqrt{\dot{\mu}_r}H_n^{(2)'}(\beta_0 a)\hat{J}_n'\left(\dot{\beta}_d a\right)}a_n
\end{aligned}
$$

2.2. Maxwell's curl equations

Microwaves or radar signals can be expressed by Maxwell's equations, which relate the electric and magnetic field values at a certain point in space and at a certain time. The differential Maxwell equations for the time-domain, which are necessary to determine the behaviour in the time-domain can be written as follows:

$$
\begin{aligned}
\nabla\times\mathbf{H} &= \frac{\partial\mathbf{D}}{\partial t}+\mathbf{J} \\
\nabla\times\mathbf{E} &= -\frac{\partial\mathbf{B}}{\partial t}-\mathbf{M} \\
\nabla.\mathbf{D} &= \rho_e \\
\nabla.\mathbf{B} &= \rho_m
\end{aligned}
\tag{2.8}
$$

where **H** is the magnetic field strength (Amperes/m or A/m), **D** is the electric displacement (Coulombs/m2 or C/m2), **E** is the electric field strength (Volts/m or V/m), **B** is the magnetic flux density (webers/ m2), **J** is the electric current density (Amperes/ m2), **M** is the magnetic current density (V/ m2), ρ_e is the electric charge density (C/m3), ρ_m is the magnetic charge density (webers/m3). The quantities given here are real functions of positions and time. In order to characterize the medium in which the electromagnetic wave interacts and to supplement Maxwell's equations, it is necessary to define the constitutive relations. The constitutive relations for isotropic, non-dispersive, and linear media can be defined as follows:

$$
\begin{aligned}
\mathbf{D} &= \varepsilon\mathbf{E}=\varepsilon_0\varepsilon_r\mathbf{E} \\
\mathbf{B} &= \mu\mathbf{H}=\mu_0\mu_r\mathbf{H}
\end{aligned}
\tag{2.9}
$$

where ε is the electric permittivity of the medium (farads/m or F/m), $\varepsilon_0 = 8.8542\times10^{-12}$(F/m) is the permittivity of free space and ε_r is the relative permittivity of the medium, μ is the magnetic permeability of the medium (henrys/m or H/m), $\mu_0 = 4\pi\times10^{-7}$(H/m) is the permeability of free space and μ_r is the relative permeability of the medium. **J** electric current density is the sum of the $\mathbf{J}_c=\sigma\mathbf{E}$ conduction current density and $\mathbf{J}_{source}$ source current density ($\mathbf{J}=\mathbf{J}_{source}+\mathbf{J}_c$). Similarly, $\mathbf{M}=\mathbf{M}_c+\mathbf{M}_{source}$ magnetic current density is the sum of $\mathbf{M}_c=\sigma^*\mathbf{H}$ and $\mathbf{M}_{source}$. σ is electric conductivity (siemens/meter), σ^* is equivalent magnetic loss (ohms/meter). Finally, by substituting the Eq. (2.9) in the Eq. (2.8) respectively and rearranging the equations, Maxwell's curl equations for lossy, linear, nondispersive, and isotropic materials can be obtained as follows:

$$
\begin{aligned}
\frac{\partial\mathbf{H}}{\partial t} &= -\frac{1}{\mu}\nabla\times\mathbf{E}-\frac{1}{\mu}\left(\mathbf{M}_{source}+\sigma^*\mathbf{H}\right) \\
\frac{\partial\mathbf{E}}{\partial t} &= \frac{1}{\varepsilon}\nabla\times\mathbf{H}-\frac{1}{\varepsilon}\left(\mathbf{J}_{source}+\sigma\mathbf{E}\right)
\end{aligned}
\tag{2.10}
$$

Six scalar equations can be obtained by writing out the vector components of Eq. (2.10) for E_x, E_y, E_z, H_x, H_y and H_z in the Cartesian coordinate system. Since Eq. (2.9) equations showing electric and magnetic charges are a direct result of curl equations, they do not need to be used in the FDTD algorithm. In other words, since both divergence equations can be obtained from curl equations and initial boundary conditions, the starting point of the FDTD algorithm is Maxwell's curl equations [24].

$$
\begin{aligned}
\frac{\partial H_x}{\partial t} &= \frac{1}{\mu}\left[\frac{\partial E_y}{\partial z}-\frac{\partial E_z}{\partial y}-\left(M_{source_x}+\sigma^*H_x\right)\right] \\
\frac{\partial H_y}{\partial t} &= \frac{1}{\mu}\left[\frac{\partial E_z}{\partial x}-\frac{\partial E_x}{\partial z}-\left(M_{source_y}+\sigma^*H_y\right)\right] \\
\frac{\partial H_z}{\partial t} &= \frac{1}{\mu}\left[\frac{\partial E_x}{\partial y}-\frac{\partial E_y}{\partial x}-\left(M_{source_z}+\sigma^*H_z\right)\right]
\end{aligned}
\tag{2.11}
$$

$$\begin{aligned}
\frac{\partial E_x}{\partial t} &= \frac{1}{\varepsilon}\left[\frac{\partial H_z}{\partial y} - \frac{\partial H_y}{\partial z} - (J_{source_x} + \sigma E_x)\right] \\
\frac{\partial E_y}{\partial t} &= \frac{1}{\varepsilon}\left[\frac{\partial H_x}{\partial z} - \frac{\partial H_z}{\partial x} - \left(J_{source_y} + \sigma E_y\right)\right] \\
\frac{\partial E_z}{\partial t} &= \frac{1}{\varepsilon}\left[\frac{\partial H_y}{\partial x} - \frac{\partial H_x}{\partial y} - \left(J_{source_z} + \sigma^* E_z\right)\right]
\end{aligned} \tag{2.12}$$

From the six equations, which are the scalar components of these rotational equations, two main groups of equations that can be evaluated independently of each other are obtained. The group containing E_x, E_y and H_z components is called the transverse electric (TE) mode, and the group containing H_x, H_y and E_z is called the transverse magnetic (TM) mode. EM waves operating in TE mode are called TE waves and EM waves operating in TM mode are called TM waves [25].

2.3. Finite difference time domain method (FDTD)

Analytical methods may not be sufficient to investigate the interaction of electromagnetic wave with an object. As stated in Analytical Study Section, it is analytically possible to examine the scattering or propagation of electromagnetic waves from a smooth surface structure such as a sphere but using numerical methods in cases where the geometry is not smooth allows us to make inferences about the wave-structure interaction. Simulating the interaction of EM waves with a structure whose material properties and geometric shapes are known is a forward problem and this forward problem can be solved using the FDTD technique. The FDTD technique can be used to obtain numerical solutions of Maxwell's equations, which can be written in differential form. In the first step, the FDTD algorithm decomposes the problem geometry into a spatial grid in which the electric and magnetic field components are placed at certain separate locations in space. In the second step, Maxwell's equations are solved in discrete time steps over time. A rectangular grid is used for the discretization because it offers advantages such as ease of use and simplicity. To satisfy Maxwell's divergence equations, the fields are first assumed to be zero throughout the computation domain. As in analytical solutions, boundary conditions apply to the outer boundary of the computational field on all dielectric and conductive surfaces. Electric and magnetic fields are continuous at the interfaces between dielectric materials. Electric and magnetic fields are calculated as a function of time in a leap-frog manner at each gridded point of the computation domain. First the electric field and then the magnetic field are calculated sequentially, and this calculation is repeated at each time step [25,26].
Somewhat surprisingly, since the transverse field representations are best understood in two dimensions [27], Maxwell's equations will be studied by transforming them into two sets of two-dimensional scalar equations. Assuming that the two-dimensional medium is the xy-plane, the problem is independent of the z-dimension, so the derivative terms for the z-dimension are vanished. By using the field distributions and the problem geometry invariance in one of the dimensions in Eq. (2.11) and Eq. (2.12), the following equations for TEz mode (given in Eq. (2.13) and TMz mode (given in Eq. (2.14)) can be obtained respectively:

$$\begin{aligned}
\frac{\partial E_x}{\partial t} &= \frac{1}{\varepsilon}\left[\frac{\partial H_z}{\partial y} - (J_{source_x} + \sigma E_x)\right] \\
\frac{\partial E_y}{\partial t} &= \frac{1}{\varepsilon}\left[-\frac{\partial H_z}{\partial x} - \left(J_{source_y} + \sigma E_y\right)\right] \\
\frac{\partial H_z}{\partial t} &= \frac{1}{\mu}\left[\frac{\partial E_x}{\partial y} - \frac{\partial E_y}{\partial x}\left(M_{source_z} + \sigma^* H_z\right)\right]
\end{aligned} \tag{2.13}$$

$$\begin{aligned}
\frac{\partial H_x}{\partial t} &= \frac{1}{\mu}\left[-\frac{\partial E_z}{\partial y} - (M_{source_x} + \sigma^* H_x)\right] \\
\frac{\partial H_y}{\partial t} &= \frac{1}{\mu}\left[\frac{\partial E_z}{\partial x} - \left(M_{source_y} + \sigma^* H_y\right)\right] \\
\frac{\partial E_z}{\partial t} &= \frac{1}{\varepsilon}\left[\frac{\partial H_y}{\partial x} - \frac{\partial H_x}{\partial y}\left(J_{source_z} + \sigma E_z\right)\right]
\end{aligned} \tag{2.14}$$

The two-dimensional, time-dependent Maxwell equations described above can be expressed discretely in space and time using the second-order exact central difference formula. The electric and magnetic field components are sampled in discrete position in space and time. In order to create a grid with the FDTD algorithm, the problem geometry is divided into cells called Yee cells. Electric field components are sampled at $0, \Delta t, 2\Delta t, ..., n\Delta t ...$ time steps, with Δt being the time sampling period, while magnetic field components are sampled at $1/2\Delta t, (1+1/2\Delta t), ..., (n+1/2\Delta t), ...$ time steps. Derivatives in Eq. (2.13) can be approximated using the central difference formula, assuming the center point of the central difference formula in space, $E_x(i, j+1/2)$, and using the center point in the time instant $(n+1/2\Delta t)$.

$$\frac{E_x|^{n+1}_{i+1/2,j} - E_x|^{n}_{i+1/2,j}}{\Delta t} = \frac{1}{\varepsilon_{i+1/2,j}}\left(\frac{H_z|^{n+1/2}_{i+1/2,j+1/2} - H_z|^{n+1/2}_{i+1/2,j-1/2}}{\Delta y} - \left(J_{source_x}|^{n+1/2}_{i+1/2,j} - \sigma_{i+1/2,j}\ E_x|^{n+1/2}_{i+1/2,j+1/2}\right)\right)$$

The $E_x|^{n+1/2}_{i+1/2,j}$ term can be written as the average of the electric fields at the $(n+1)\Delta t$ and $n\Delta t$ time steps as follows:

$$E_x|^{n+1/2}_{i+1/2,j+1/2} = \frac{E_x|^{n+1}_{i+1/2,j+1/2} + E_x|^{n}_{i+1/2,j+1/2}}{2}$$

$$E_x|_{i+1/2\,,j}^{n+1} - E_x|_{i+1/2\,,j}^{n} = \frac{\Delta t}{\varepsilon_{i,j+1/2}}\left(\frac{H_z|_{i+1/2\,,j+1/2}^{n+1/2} - H_z|_{i+1/2\,,j-1/2}^{n+1/2}}{\Delta y} - \left(J_{source_x}|_{i+1/2\,,j}^{n+1/2} - \sigma_{i+1/2\,,j}\left(\frac{E_x|_{i+1/2\,,j+1/2}^{n+1} + E_x|_{i+1/2\,,j+1/2}^{n}}{2}\right)\right)\right) \quad (2.15)$$

When the terms with the same index are collected to the same side and the Eq. (2.15) can be written according to $E_x|_{i+1/2\,,j}^{n+1}$ as Eq. (2.16).

$$\left(1 + \frac{\sigma_{i+1/2\,,j}\Delta t}{2\varepsilon_{i+1/2\,,j}}\right) E_x|_{i+1/2\,,j}^{n+1} = \left(1 - \frac{\sigma_{i+1/2\,,j}\Delta t}{2\varepsilon_{i+1/2\,,j}}\right) E_x|_{i+1/2\,,j}^{n} + \frac{\Delta t}{\varepsilon_{i+1/2\,,j}}\left(\frac{H_z|_{i+1/2\,,j+1/2}^{n+1/2} - H_z|_{i+1/2\,,j-1/2}^{n+1/2}}{\Delta y} - J_{source_x}|_{i+1/2\,,j}^{n+1/2}\right) \quad (2.16)$$

Dividing both sides of the Eq. (2.16) by $\left(1 + \sigma_{i,j+1/2}\,\Delta t/2\varepsilon_{i,j+1/2}\right)$ explicit update equation for $E_x|_{i,j+1/2}^{n+1}$ can be obtained as Eq. (2.17):

$$\begin{aligned} E_x|_{i+1/2\,,j}^{n+1} &= \left(\frac{2\varepsilon_{i+1/2,j} - \sigma_{i+1/2\,,j}\Delta t}{2\varepsilon_{i+1/2\,,j} + \sigma_{i+1/2,j}\,\Delta t}\right) E_x|_{i+1/2\,,j}^{n} \\ &+ \left(\frac{2\Delta t}{\left(2\varepsilon_{i+1/2,j} + \sigma_{i+1/2\,,j}\Delta t\right)\Delta y}\right)\left(H_z|_{i+1/2\,,j+1/2}^{n+1/2} - H_z|_{i+1/2\,,j-1/2}^{n+1/2}\right) \\ &- \left(\frac{2\Delta t}{2\varepsilon_{i+1/2,j} + \sigma_{i+1/2\,,j}\Delta t}\right) J_{source_x}|_{i+1/2\,,j}^{n+1/2} \end{aligned} \quad (2.17)$$

Similarly, the explicit update equations for $E_y|_{i,j+1/2}^{n+1}$ and $H_z|_{i+1/2\,,j+1/2}^{n+1/2}$ can also be obtained as in Eq. (2.18) and Eq. (2.19), respectively.

$$\begin{aligned} E_y|_{i,j+1/2}^{n+1} &= \left(\frac{2\varepsilon_{i,j+1/2} - \sigma_{i,j+1/2}\,\Delta t}{2\varepsilon_{i,j+1/2} + \sigma_{i,j+1/2}\,\Delta t}\right) E_y|_{i,j+1/2}^{n} \\ &+ \left(\frac{2\Delta t}{\left(2\varepsilon_{i,j+1/2} + \sigma_{i,j+1/2}\,\Delta t\right)\Delta x}\right)\left(H_z|_{i-1/2\,j+1/2}^{n+1/2} - H_z|_{i+1/2\,,j+1/2}^{n+1/2}\right) \\ &- \left(\frac{2\Delta t}{2\varepsilon_{i,j+1/2} + \sigma_{i,j+1/2}\,\Delta t}\right) J_{source_y}|_{i,j+1/2}^{n+1/2} \end{aligned} \quad (2.18)$$

$$\begin{aligned} H_z|_{i+1/2\,,j+1/2}^{n+1/2} &= \left(\frac{2\mu_{i+1/2\,,j+1/2} - \sigma_{i+1/2\,,j+1/2}\,\Delta t}{2\mu_{i+1/2\,,j+1/2} + \sigma_{i+1/2\,,j+1/2}\,\Delta t}\right) H_z|_{i+1/2\,,j+1/2}^{n-1/2} \\ &+ \left(\frac{2\Delta t}{\left(2\mu_{i+1/2\,,j+1/2} + \sigma_{i+1/2\,,j+1/2}\,\Delta t\right)\Delta y}\right)\left(E_x|_{i+1/2\,,j+1}^{n} - E_x|_{i+1/2\,,j}^{n}\right) \\ &- \left(\frac{2\Delta t}{\left(2\mu_{i+1/2\,,j+1/2} + \sigma_{i+1/2\,,j+1/2}\,\Delta t\right)\Delta x}\right)\left(E_y|_{i+1,j+1/2}^{n} - E_y|_{i,j+1/2}^{n}\right) \\ &- \left(\frac{2\Delta t}{2\mu_{i+1/2\,,j+1/2} + \sigma_{i+1/2\,,j+1/2}\,\Delta t}\right) M_{source_z}|_{i+1/2\,,j+1/2}^{n} \end{aligned} \quad (2.19)$$

In here, the FDTD update equations of the field components of the TEz mode are obtained, and the update equations of the field components of the TMz mode can be calculated in a similar way.

2.4. Alternating direct implicit- FDTD (ADI-FDTD)

In this study, subgrids that use finer spatial resolution can be used in the numerical modeling of breast tissue and electromagnetic wave interaction, especially in parts with tumors. By using these subgrids, certain regions of the computational field with high dielectric constant can be modeled in detail and the propagation of short wavelength waves can be better represented. By combining the standard FDTD method with the unconditionally stable ADI-FDTD technique, a finer grid and thus more effective simulation results can be obtained in a certain region of the FDTD computation domain. ADI-FDTD is unconditionally stable so that by setting the time step to any value, FDTD can be used in parts with low dielectric value and ADI-FDTD in places with high dielectric value in the same computation region without using a time interpolation scheme. Since the standard FDTD method is an explicit finite difference algorithm, the Courant–Friedrich–Levy (CFL) stability condition must be satisfied. According to CFL condition, a small-time step size results in a significant increase in computation time when using a smaller cell size compared to the wavelength, since the size of the time step should not exceed the minimum cell size in the computation domain. The constraint of the CFL condition can be overcome with the ADI-FDTD algorithm applied to the Yee algorithm to solve Maxwell's equations. The numerical formulation of the ADI-FDTD method for a 2-D TE wave is presented in Eq. (2.20)-(2.22), and the electromagnetic field components are arranged on the cells as in the standard FDTD method. The reason why both standard FDTD and ADI-FDTD algorithms are used together is to obtain a better simulation result by using a finer grid to the computation domain corresponding to the tumor tissue whose location is determined by the FDTD method. The smaller cell is not used in the entire ADI-FDTD calculation

region. The standard FDTD algorithm and cell size are used in the healthy breast tissue portion of the computation domain. Electric fields at the main grid-local grid (the area with smaller cells) are calculated by interpolating the fields in the main grid, and the fields in the local grid are calculated with the ADI-FDTD algorithm. The ADI-FDTD update equations for a 2-D TE wave are arranged on cells as in the standard FDTD method and presented below:

$$\begin{aligned} E_x|_{i+1/2,j}^{n+1/2} &= \left(\frac{2\varepsilon_{i+1/2,j} - \sigma_{i+1/2,j}\Delta t}{2\varepsilon_{i+1/2,j} + \sigma_{i+1/2,j}\Delta t}\right) E_x|_{i+1/2,j}^{n} \\ &+ \left(\frac{2\Delta t}{\left(2\varepsilon_{i+1/2,j} + \sigma_{i+1/2,j}\Delta t\right)\Delta y}\right)\left(H_z|_{i+1/2,j+1/2}^{n} - H_z|_{i+1/2,j-1/2}^{n}\right) \\ &- \left(\frac{2\Delta t}{2\varepsilon_{i+1/2,j} + \sigma_{i+1/2,j}\Delta t}\right) J_{source_x}|_{i+1/2,j}^{n} + \end{aligned} \tag{2.20}$$

$$\begin{aligned} E_y|_{i,j+1/2}^{n+1/2} &= \left(\frac{2\varepsilon_{i,j+1/2} - \sigma_{i,j+1/2}\Delta t}{2\varepsilon_{i,j+1/2} + \sigma_{i,j+1/2}\Delta t}\right) E_y|_{i,j+1/2}^{n} \\ &+ \left(\frac{2\Delta t}{\left(2\varepsilon_{i,j+1/2} + \sigma_{i,j+1/2}\Delta t\right)\Delta x}\right)\left(H_z|_{i-1/2\,j+1/2}^{n+1/2} - H_z|_{i+1/2,j+1/2}^{n+1/2}\right) \\ &- \left(\frac{2\Delta t}{2\varepsilon_{i,j+1/2} + \sigma_{i,j+1/2}\Delta t}\right) J_{source_y}|_{i,j+1/2}^{n} + \end{aligned} \tag{2.21}$$

$$\begin{aligned} H_z|_{i+1/2,j+1/2}^{n+1/2} &= \left(\frac{2\mu_{i+1/2,j+1/2} - \sigma_{i+1/2,j+1/2}\Delta t}{2\mu_{i+1/2,j+1/2} + \sigma_{i+1/2,j+1/2}\Delta t}\right) H_z|_{i+1/2,j+1/2}^{n} \\ &+ \left(\frac{2\Delta t}{\left(2\mu_{i+1/2,j+1/2} + \sigma_{i+1/2,j+1/2}\Delta t\right)\Delta y}\right)\left(E_x|_{i+1/2,j+1}^{n} - E_x|_{i+1/2,j}^{n}\right) \\ &- \left(\frac{2\Delta t}{2\mu_{i+1/2,j+1/2} + \sigma_{i+1/2,j+1/2}\Delta t}\right)\left(E_y|_{i+1,j+1/2}^{n+1/2} - E_y|_{i,j+1/2}^{n+1/2}\right) \\ &- \left(\frac{2\Delta t}{2\mu_{i+1/2,j+1/2} + \sigma_{i+1/2,j+1/2}\Delta t}\right) M_{source_z}|_{i+1/2,j+1/2}^{n} + \end{aligned} \tag{2.22}$$

The set of Eq. (2.17)-(2.19) applies to a coarse grid region, while the set of Eq. (2.20)-(2.22) applies to a finer grid region. For the interface between the two regions, an interpolation scheme required only in space is applied, since the same time step is used in both thick and thin meshes.

2.5. Dielectric properties of breast tissues

Microwave imaging is a technique that uses microwaves to detect objects embedded or hidden in a medium. The main argument for this technique is the significant difference in the dielectric properties of cancerous tumors compared to healthy tissues. Field distribution imaging using microwaves is based on the variation of dielectric properties between normal breast tissue and tumor tissue at microwave frequencies. In order to understand the interaction between microwaves and breast tissue, it is necessary to know the dielectric properties of breast tissues [37, 38]. Studies have been carried out to measure the dielectric properties of cancerous tissues in various tissue types in the radio and microwave frequency ranges in the 10 Hz-20 GHz frequency range, and it has been observed that the dielectric properties of cancerous tissues are different from healthy tissues. The dielectric properties of breast tissues are represented by a complex relative permittivity. $\varepsilon = \varepsilon' - j\varepsilon''$. The real part of this complex number representing the ability of the material to store microwave energy, while the imaginary part indicates the ability of the material to absorb microwave energy and is also called the loss factor. σ is the electrical conductivity of the sample, ω is the angular frequency of the field, ε_0 is the permittivity of free space and $\varepsilon'' = \sigma/\omega\varepsilon_0$.
Measurements in the radio and microwave range have shown that the dielectric properties of healthy breast tissue differ significantly in the vicinity of malignant breast tissues. The results obtained as a result of the measurements vary depending on the number of samples used, the detection volume and depth, the frequency range, and the size of the tissue [39, 40]. Although there are $\pm 10^{0}/_{0}$ differences between the measurement values of the dielectric properties of breast tissues at microwave frequencies, the average values are as in Table 2.1.

3. Numerical Results and Discussions

Two different simulation setups have been developed to observe the interaction of electromagnetic waves at microwave frequencies and breast tissue. These simulation setups form the computational domain of our numerical approach, and calculations are made using the FDTD and ADI-FDTD technique. While solving with the FDTD method, the space should be truncated in a certain place where it will be sufficient in terms of interactions. After the computation domain is determined, the PML absorbing boundary condition is used from the truncated region to model the real infinity and it is assumed that the PML layer surrounds all of the computation domain.

Mediums	ε_r	$\sigma_s\,(S/m)$	μ_r
Normal Breast Tissue	9.0	0.4	1.0
Skin	36.0	4.0	1.0
Malignant	50.0	7.0	1.0
Air	1.0	0.0	1.0

Table 2.1: Parameters of the mediums [37]

3.1. Preparation of the simulation setup

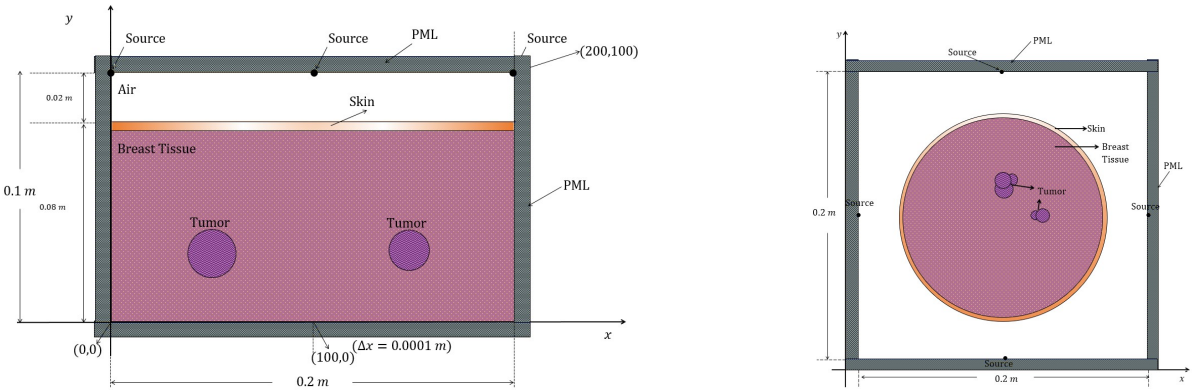

Figure 3.1: **(a)** Rectangular breast model, **(b)** Spherical breast model

In Figure 3.1a a rectangular computational domain is given. The length of the computation region on the x-axis is 0.2 m and the length on the y-axis is 0.1 m. Along the y-axis, 0.076 is breast tissue, 0.004 is skin and 0.02 is air. In the computation domain two tumor tissues in the form of circles with diameters 0.018 m and 0.015 m, which accept the points (0.12, 0.03), (0.16, 0.03) of the computation domain as centers, respectively, are defined. In Figure 3.1b, it is assumed that there is a circular breast tissue inside a square computational domain. The diameter of the circular breast tissue is accepted as 0.16 m and the thickness of the skin layer is taken as 0.004 m, which corresponds to four-unit cells in the FDTD computation space. It is accepted that cancerous tissues are concentrated in two different locations in the circular region and the tumor is expressed using circles whose centers are very close to each other. The first concentration of cancerous tissues is in the upper half of the computation domain, and three circles close to each other are used, and their diameters and coordinates are as follows, respectively: 0.01 m, 0.014 m, 0.016 m and (0.1,0.13), (0.1,0.12), (0.11,0.13). The second concentration of cancerous tissues is in the right side of the computation domain, and two circles close to each other are used, and their diameters and coordinates are as follows, respectively: 0.008 m, 0.012 m, and (0.12,0.1), (0.128,0.1), (0.11,0.13). It is assumed that all cells in the computation domain are the same size The simulation setup and computation domain dimensions are given in Figure 3.1 in detail.

3.2. Simulation results

Sources are the components that initiate the finite difference simulation by activating the electric and magnetic fields as a function of time. Although sources are divided into far field and near field depending on the type of problem being solved, the frequency spectrum of the selected source waveform should be chosen so that all frequencies are considered in the simulations. The frequency range at which valid and accurate simulation results can be obtained is determined by the frequency spectrum of the source waveform. Since frequency and wavelength are inversely proportional, the highest frequency in the source waveform spectrum must be smaller than the highest frequency-wavelength ratio of the cell size. Since the Gaussian waveform can be created to cover all frequencies up to the highest frequency, which depends on the cell size by a factor, the Gaussian waveform is used for the simulations.

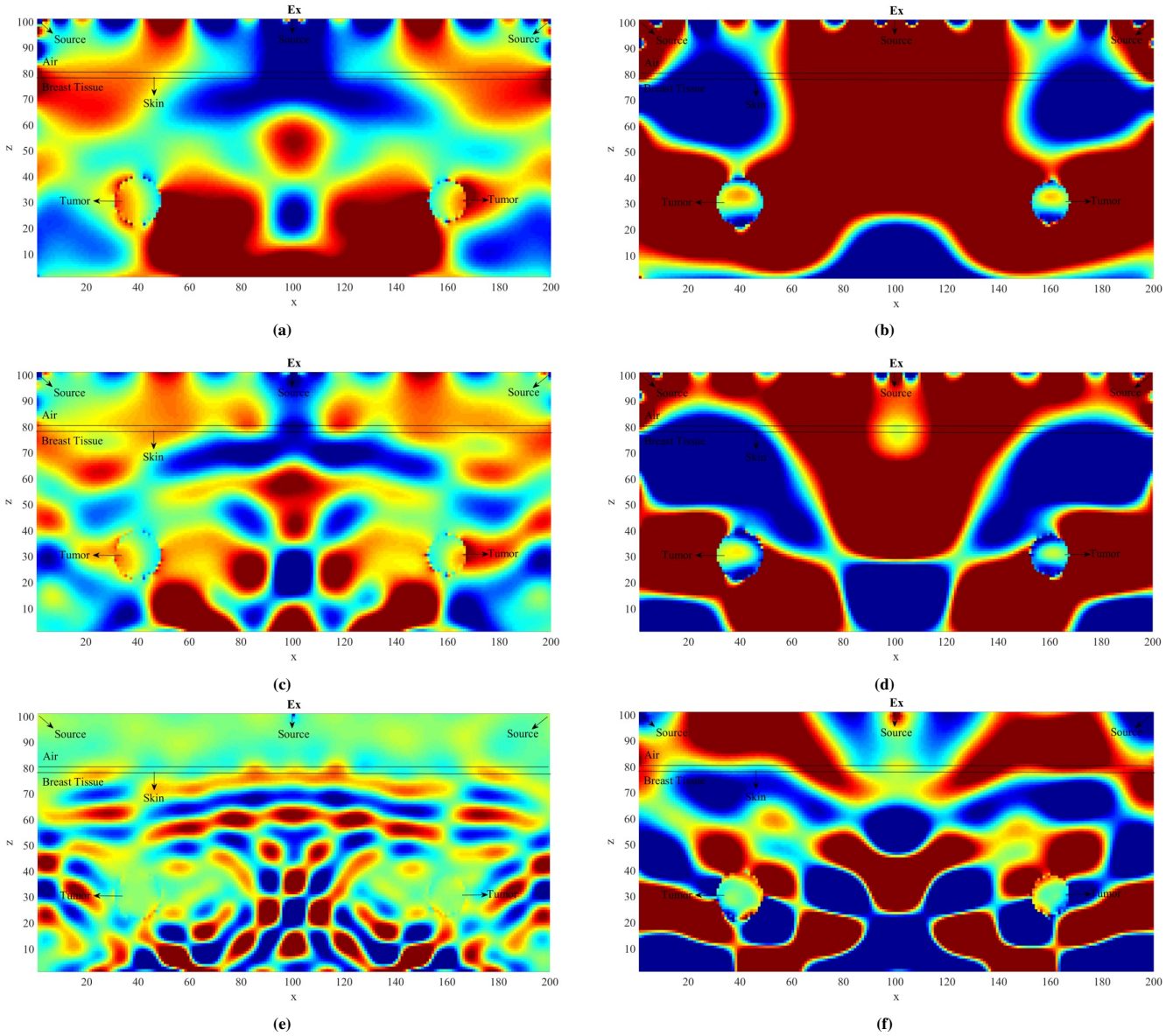

Figure 3.2: Simulation result for rectangular breast model for 650-time step: **(a)** Ex field distribution at 1.5 GHz by FDTD algorithm, **(b)** Ex field distribution at 1.5 GHz by ADI-FDTD algorithm, **(c)** Ex field distribution at 3.0 GHz by FDTD algorithm, **(d)** Ex field distribution at 3.0 GHz by ADI-FDTD algorithm, **(e)** Ex field distribution at 6.0 GHz by FDTD algorithm, **(f)** Ex field distribution at 6.0 GHz by ADI-FDTD algorithm

In Figure 3.2 and Figure 3.3 rectangular simulation setup results are obtained and presented. The Ex-field distributions of the TE mode are presented in using both FDTD and ADI-FDTD algorithms. In the TE wave simulation results obtained using the FDTD algorithm, when the states of the images at different frequencies are compared, better results are obtained at 1.5 GHz frequency. At 3.0 GHz frequency, tumor tissue is less prominent than at 1.5 GHz, and tumor tissue is almost invisible at 6.0 GHz. The Ez-field distributions of the TM mode are presented in Figure 3.3 using both FDTD and ADI-FDTD algorithms. In Figure 3.3, similar to Figure 3.2, 1.5 GHz frequency gives better results in the simulation results obtained using the FDTD algorithm.

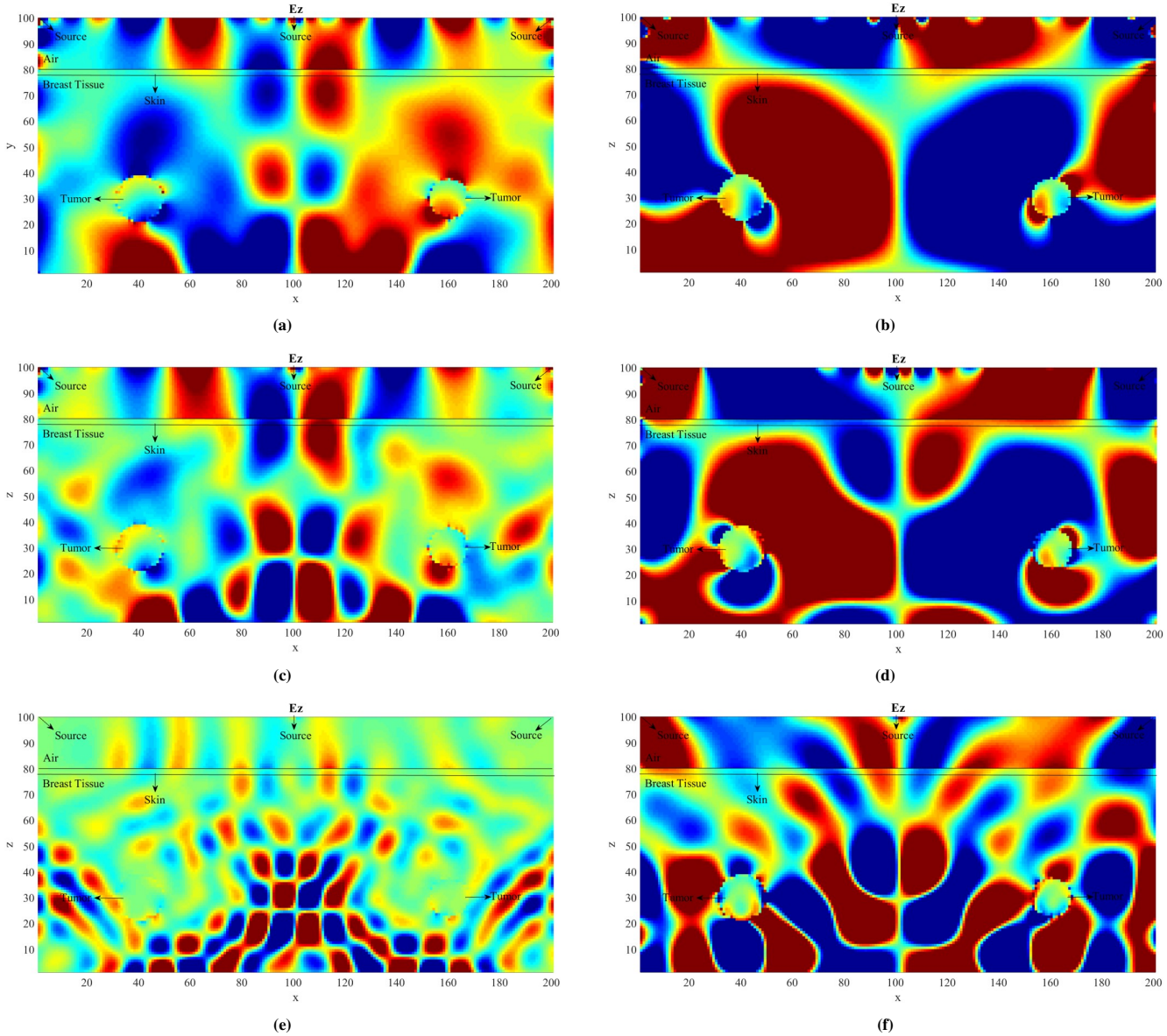

Figure 3.3: Simulation result for rectangular breast model for 650-time step: **(a)** Ez field distribution at 1.5 GHz by FDTD algorithm, **(b)** Ez field distribution at 1.5 GHz by ADI-FDTD algorithm, **(c)** Ez field distribution at 3.0 GHz by FDTD algorithm, **(d)** Ez field distribution at 3.0 GHz by ADI-FDTD algorithm, **(e)** Ez field distribution at 6.0 GHz by FDTD algorithm, **(f)** Ez field distribution at 6.0 GHz by ADI-FDTD algorithm

Circular breast model with massive tumor tissue is modeled in Figure 3.4 and Figure 3.5, Ex field distribution for TE mode and Ez field distribution for TM mode are presented respectively.

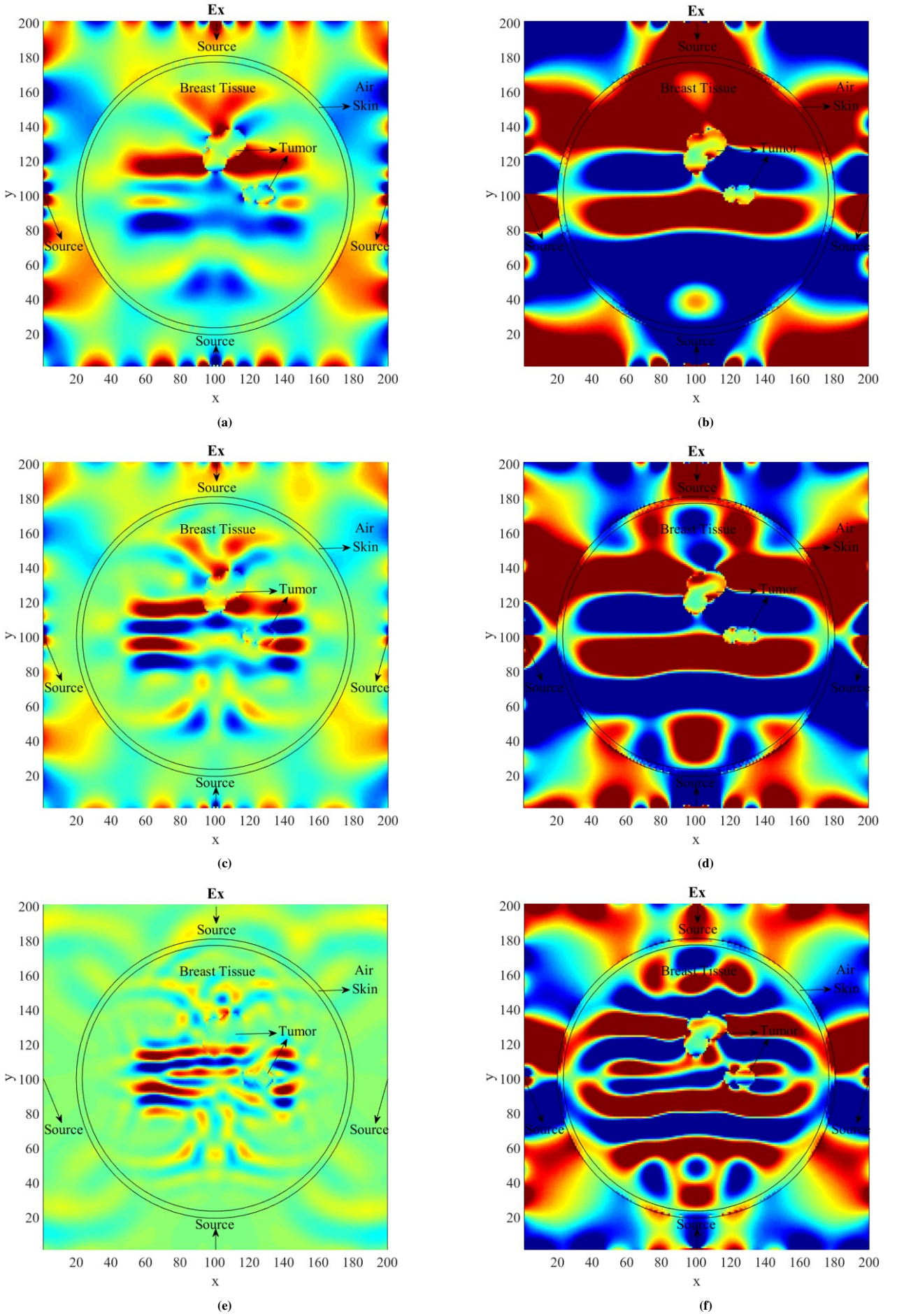

Figure 3.4: Simulation result for spherical breast model for 650-time step: **(a)** Ex field distribution at 1.5 GHz by FDTD algorithm, **(b)** Ex field distribution at 1.5 GHz by ADI-FDTD algorithm, **(c)** Ex field distribution at 3.0 GHz by FDTD algorithm, **(d)** Ex field distribution at 3.0 GHz by ADI-FDTD algorithm, **(e)** Ex field distribution at 6.0 GHz by FDTD algorithm, **(f)** Ex field distribution at 6.0 GHz by ADI-FDTD algorithm

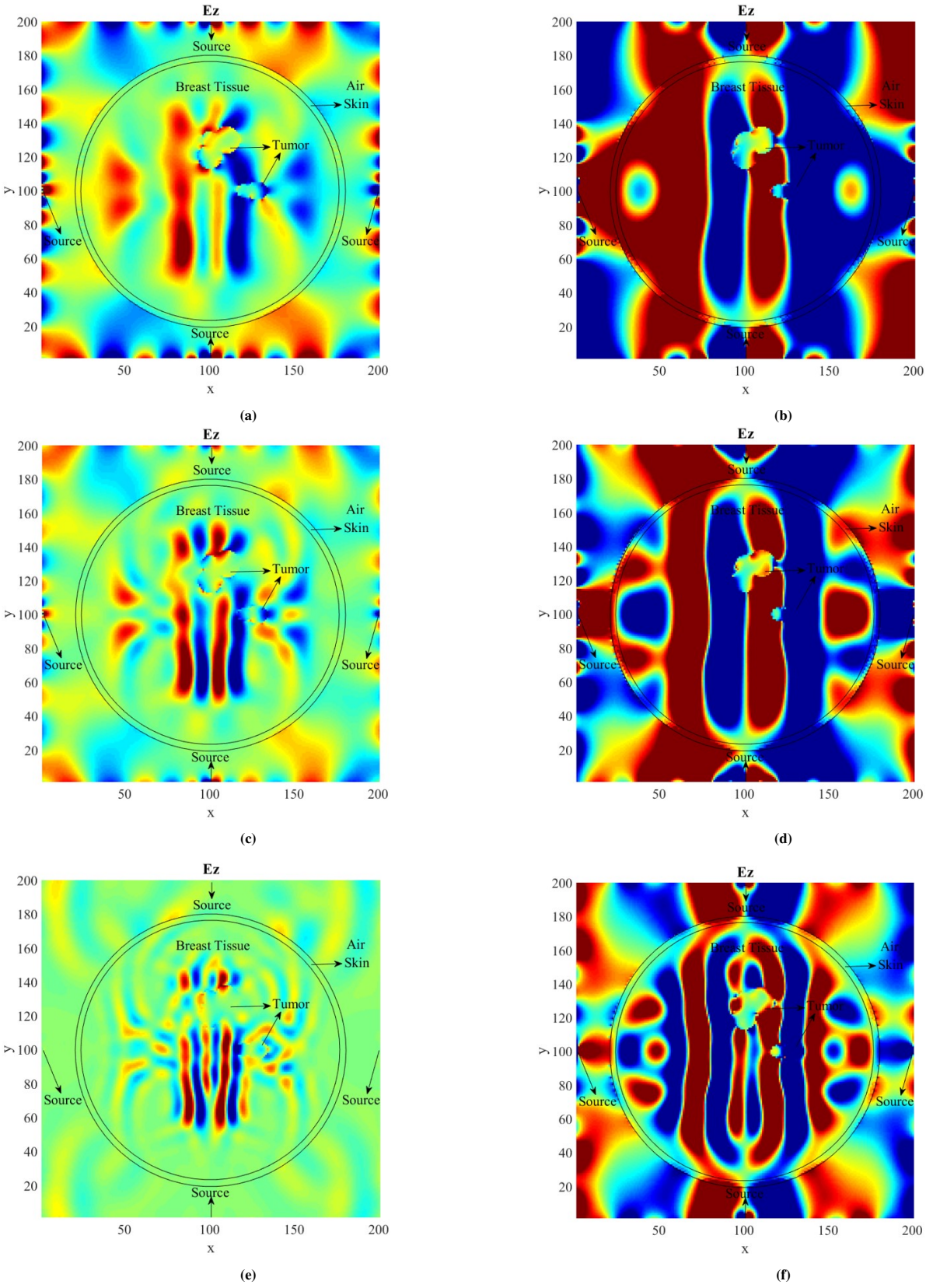

Figure 3.5: Simulation result for spherical breast model for 600-time step: **(a)** Ez field distribution at 1.5 GHz by FDTD algorithm, **(b)** Ez field distribution at 1.5 GHz by ADI-FDTD algorithm, **(c)** Ez field distribution at 3.0 GHz by FDTD algorithm, **(d)** Ez field distribution at 3.0 GHz by ADI-FDTD, **(e)** Ez field distribution at 6.0 GHz by FDTD algorithm, **(f)** Ez field distribution at 6.0 GHz by ADI-FDTD algorithm

Since the geometric structure of the tumor tissue is more complex in the circular model, the boundaries of the tumor tissue are not clear even at the frequency of 3.0 GHz. In the simulation results obtained using the FDTD algorithm, the best result was obtained at the 1.5 GHz frequency. In the results obtained with the help of the ADI-FDTD algorithm, tumor tissue can be observed at all three frequencies. When the Ex and Ez field distributions are compared, since there is more scattering of the wave in the Ez field distribution, the transition of the medium wave to a different medium is observed more clearly.

4. Conclusion

The propagation of electromagnetic waves varies depending on the dielectric properties of the medium. Depending on the dielectric properties of the medium, there may be there may be scattering, lossy propagation, and attenuation may occur. The dielectric properties of cancerous tissue differ significantly from those of healthy tissues. Since the different dielectric properties affect the propagation of the wave, the position and shape of the cancerous breast tissues are modeled mathematically by using the electromagnetic field distribution in the breast tissue. The mathematical modeling of the interaction of waves with mediums can be presented using Maxwell's equations. When the geometry of the interacting medium is smooth, the field distribution in the medium can be calculated analytically. Since cancer tissue is a lossy medium, its shape is assumed to be spherical and the field distribution of electromagnetic waves in the lossy dielectric sphere is calculated analytically. When the medium in which the wave propagates is geometrically complex, the field distribution can be determined by numerical methods. In this study, the shape and location of the tumor are determined using the FDTD method, which is a widely used method for computing the propagation of electromagnetic waves. The propagation of the wave in the breast tissue and the distribution of the fields are simulated with FDTD algorithm. After determining the location of the tumor, better simulation results are obtained by using ADI-FDTD to the location of the tumor and FDTD to the region of healthy tissues. Using both TE and TM waves, the field distributions of waves with different polarizations are compared. In the simulations, both the Ex-field distribution of the TE mode and the Ez field distribution of the TM mode are obtained, and the simulation results obtained at the center frequency of L (1.0-2.0 GHz), S (2.0-4.0 GHz) and C (4.0-8.0 GHz) bands using the FDTD and ADI-FDTD algorithms are compared. In the results obtained using the ADI-FDTD algorithm, tumor tissue is observed more clearly. In the Ez-field distributions, the propagation of the wave from the air medium to the breast tissue can be observed more clearly. Although generally better results are obtained in lower frequency bands, the best results are obtained at 1.5 GHz frequency with the help of ADI-FDTD hybrid algorithm. Using the established mathematical model, it has been shown that the detection of breast cancer can be made with the help of the field distributions obtained as a result of the propagation of electromagnetic waves.

Article Information

Acknowledgements: The authors would like to express their sincere thanks to the editor and the anonymous reviewers for their helpful comments and suggestions.

Author's contributions: The article has a single author. The author has read and approved the final manuscript.

Conflict of interest disclosure: No potential conflict of interest was declared by the author.

Supporting/Supporting organizations: No grants were received from any public, private or non-profit organizations for this research.

Ethical approval and participant consent: It is declared that during the preparation process of this study, scientific and ethical principles were followed and all the studies benefited from are stated in the bibliography.

Plagiarism statement: This article was scanned by the plagiarism program. No plagiarism detected.

Availability of data and materials: Not applicable.

References

[1] F. Bray, M. Laversanne, E. Weiderpass, I. Soerjomataram, *The ever-increasing importance of cancer as a leading cause of premature death worldwide,* Cancer, **127** (16) (2021), 3029-3030.
[2] W. Organization, *Global Health Estimates 2019: deaths by cause, age, sex, by country and by region 2000–2019,* WHO, (2020).
[3] H. Sung, J. Ferlay, R. Siegel, M. Laversanne, I. Soerjomataram, A. Jemal, F. Bray, *Global cancer statistics 2020: GLOBOCAN estimates of incidence and mortality worldwide for 36 cancers in 185 countries,* CA: A Can. J. Clinc., **71** (3) (2021), 209-249 .
[4] M. Lu, X. Xiao, G. Liu, H. Lu, *Microwave breast tumor localization using wavelet feature extraction and genetic algorithm-neural network,* Med. Phys., **48** (10) (2021), 6080-6093.
[5] E. Bond, X. Li, S. Hagness, B. Van Veen, *Microwave imaging via space-time beamforming for early detection of breast cancer,* IEEE Trans. Anten. Prop., **51** (8) (2003), 1690-1705.
[6] M. Lazebnik, M. Okoniewski, J. Booske, S. Hagness, *Highly accurate Debye models for normal and malignant breast tissue dielectric properties at microwave frequencies,* IEEE Mic. Wirel. Comp. Lett., **17** (12) (2007), 822-824.
[7] N. Nikolova, *Microwave imaging for breast cancer,* IEEE Mic. Mag., **12** (7) (2011), 78-94.
[8] R. Conceição, J. Mohr, M. O'Halloran, (Eds.), *An Introduction to Microwave Imaging for Breast Cancer Detection,* Basel, Switzerland, Springer International Publishing, 2016.
[9] S. Kwon, S. Lee, *Recent advances in microwave imaging for breast cancer detection*, Internat. J. Biomed. Imaging, (2016), 1-26.
[10] S. Davis, B. Van Veen, S. Hagness, F Kelcz, *Breast tumor characterization based on ultrawideband microwave backscatter*, IEEE Trans. Biomed. Engrg., **55** (1) (2007), 237-246.
[11] M. Zhao, J. Shea, S. Hagness, D. Weide, B. Van Veen, T. Varghese, *Numerical study of microwave scattering in breast tissue via coupled dielectric and elastic contrasts,* IEEE Anten. Wirer. Prop. Lett., **7** (2008), 247-250.
[12] L. Wang, *Microwave imaging and sensing techniques for breast cancer detection*,Micromachines, **14** (7) (2023), 1462.
[13] R. Torrealba-Meléndez, J. Olvera-Cervantes, A. Corona-Chávez, *UWB microwave radar imaging for detection and discrimination of benign and malignant breast tumors using circularly polarized antennas*, (IEEE WAMICON 2014), (2014), 1-3.
[14] K. Noritake, S. Kidera, Accurate breast surface imaging method with FDTD-based waveform correction for microwave mammography, 2017 International Symposium On Antennas And Propagation (ISAP 2017), (2017), 1-2.
[15] A. Fhager, M. Persson, Reconstrunction strategies for microwave imaging of breast; reconstructions constrained to the breast domain, IEEE MTT-S International Microwave Bio Conference (IMBIOC 2017), (2017), 1-3.
[16] L. Wang, *Microwave sensors for breast cancer detection*, Sensors, **18** (2) (2018), 655.
[17] H. El Misilmani, T. Naous, S. Al Khatib, K. Kabalan, *A survey on antenna designs for breast cancer detection using microwave imaging,* IEEE Access, **8** (2020), 102570-102594.
[18] M. Ahadi, J. Nourinia, C. Ghobadi, *Square monopole antenna application in localization of tumors in three dimensions by confocal microwave imaging for breast cancer detection: experimental measurement*, Wirel. Pers. Commun., **116** (2021), 2391-2409.

[19] B.Moloney, D. O'Loughlin, S. Abd Elwahab, M. Kerin, *Breast cancer detection—A synopsis of conventional modalities and the potential role of microwave imaging*, Diagnostics, **10** (2) (2020), 103.

[20] D. Carvalho, A. Aragão, A. Ferrari, B.Sanches, W. Noije, Software-defined radio assessment for microwave imaging breast cancer detection, 2020 IEEE Nordic Circuits and Systems Conference (NorCAS 2020), (2020), 1-6.

[21] D. Godinho, J. Felicio, C. Fernandes, R. Conceicao, *Experimental evaluation of an axillary microwave imaging system to aid breast cancer staging*, IEEE J. Elect., RF Mic. Med. Biology, **6** (1) (2021), 68-76.

[22] C. Balanis, *Advanced Engineering Electromagnetics*, John Wiley and Sons, 2012.

[23] İ. Ünal, B. Turetken, U. Bulus, C. Canbay, Analysis of the electromagnetic field scattered by a spherical breast tumour model, 2013 International Symposium On Electromagnetic Theory, (2013), 574-577.

[24] A.Taflove, S. Hagness, M. Piket-May, *Computational electromagnetics: the finite-difference time-domain method*, Elec. Eng. Hand., **3** (15) (2005), 629-670.

[25] D. Sullivan, *Electromagnetic Simulation Using the FDTD Method*, John Wiley and Sons, 2013.

[26] K. Kunz, R. Luebbers, *The Finite Difference Time Domain Method for Electromagnetics*, CRC Press,1993.

[27] A. Elsherbeni, V. Demir, *The Finite-Difference Time-Domain Method for Electromagnetics with MATLAB® Simulations*, IET, 2015.

[28] T. Namiki, *A new FDTD algorithm based on alternating-direction implicit method*, IEEE Trans. Mic. Theory Tech., **47** (10) (1999), 2003-2007.

[29] T.Namiki, *3-D ADI-FDTD method-unconditionally stable time-domain algorithm for solving full vector Maxwell's equations*, IEEE Trans. Mic. Theory Tech., **48** (10) (2000), 1743-1748.

[30] X. Wang, J. Gao, Z. Chen, F. Teixeira, *Unconditionally stable one-step leapfrog ADI-FDTD for dispersive media*, IEEE Trans. Antenn. Prop., **67** (4) (2019), 2829-2834.

[31] D. Y. Heh, E. L. Tan, *Unconditionally stable multiple one-dimensional ADI-FDTD method for coupled transmission lines,* IEEE Trans. Antenn. Prop., **66** (12) (2018), 7488-7492.

[32] E. L. Tan, D. Y. Heh, *Multiple 1-D fundamental ADI-FDTD method for coupled transmission lines on mobile devices*, IEEE J. Multisc. Multiph. Comp. Tech., **4** (2019) 198-206.

[33] B. Zou, S. Liu, L. Zhang, S. Ren, *Efficient one-step leapfrog ADI-FDTD for far-field scattering calculation of lossy media*, Mic. Opt. Tech. Lett. 62 (5) (2020), 1876-1881.

[34] G. Mur, *Absorbing boundary conditions for the finite-difference approximation of the time-domain electromagnetic-field equations*, IEEE Trans. Elec. Comput., **4** (1981), 377-382.

[35] J. Berenger, *A perfectly matched layer for the absorption of electromagnetic waves,* J. Comput. Phys., **114** (2) (1994), 185-200.

[36] J. Berenger, *Perfectly matched layer for the FDTD solution of wave-structure interaction problems*, IEEE Trans. Antenn. Prop., **44** (1) (1996), 110-117.

[37] E. Zastrow, S. Davis, M. Lazebnik, F. Kelcz, B. Van Veen, S. Hagness, *Development of anatomically realistic numerical breast phantoms with accurate dielectric properties for modeling microwave interactions with the human breast,* IEEE Trans. Biomed. Engrg., **55** (12) (2008), 2792-2800.

[38] E. Fear, M. Stuchly, *Microwave detection of breast cancer*, IEEE Trans. Mic. Theory Tech., **48** (11) (2000), 1854-1863.

[39] S. Hagness, A. Taflove, J. Bridges, *Three-dimensional FDTD analysis of a pulsed microwave confocal system for breast cancer detection: Design of an antenna-array element*, IEEE Trans. Antenn. Prop., **47** (5) (1999), 783-791.

[40] M. Lazebnik, C. Watkins, S. Hagness, J. Booske, D. Popovic, L. McCartney, M. Okoniewski, M. Lindstrom, T. Breslin, J. Harter, The dielectric properties of normal and malignant breast tissue at microwave frequencies: analysis, conclusions, and implications from the wisconsin/calgary study, 2007 IEEE Antennas And Propagation Society International Symposium (2007), 2172-2175.